

Research Article

Open Access



A novel zero-force control framework for post-stroke rehabilitation training based on fuzzy-PID method

Lina Tong¹, Decheng Cui¹, Chen Wang², Liang Peng²

¹School of Artificial Intelligence, China University of Mining and Technology, Beijing 100083, China.

²State Key Laboratory of Multimodal Artificial Intelligence Systems, Institute of Automation, Chinese Academy of Sciences, Beijing 100090, China.

Correspondence to: Dr. Chen Wang, Dr. Liang Peng, State Key Laboratory of Multimodal Artificial Intelligence Systems, Institute of Automation, Chinese Academy of Sciences, 52 Sanlihe Rd., Xicheng District, Beijing 100190, China. E-mail: wangchen2016@iaac.cn; liang.peng@ia.ac.cn

How to cite this article: Tong L, Cui D, Wang C, Peng L. A novel zero-force control framework for post-stroke rehabilitation training based on fuzzy-PID method. *Intell Robot* 2024;4(1):125-45. <http://dx.doi.org/10.20517/ir.2024.08>

Received: 1 Dec 2023 **First Decision:** 15 Jan 2024 **Revised:** 8 Feb 2024 **Accepted:** 23 Feb 2024 **Published:** 21 Mar 2024

Academic Editor: Simon X. Yang **Copy Editor:** Pei-Yun Wang **Production Editor:** Pei-Yun Wang

Abstract

As the number of people with neurological disorders increases, movement rehabilitation becomes progressively important, especially the active rehabilitation training, which has been demonstrated as a promising solution for improving the neural plasticity. In this paper, we developed a 5-degree-of-freedom rehabilitation robot and proposed a zero-force control framework for active rehabilitation training based on the kinematics and dynamics identification. According to the robot motion characteristics, the fuzzy PID algorithm was designed to further improve the flexibility of the robot. Experiments demonstrated that the proposed control method reduced the Root Mean Square Error and Mean Absolute Error evaluation indexes by more than 15% on average and improves the coefficient of determination (R^2) by 4% compared with the traditional PID algorithm. In order to improve the active participation of the post-stroke rehabilitation training, this paper designed an active rehabilitation training scheme based on gamified scenarios, which further enhanced the efficiency of rehabilitation training by means of visual feedback.

Keywords: Upper limb exoskeleton rehabilitation robot, rehabilitation, zero force control, fuzzy control, virtual reality

1. INTRODUCTION

With the ageing of the population in society, the number of elderly people with movement disorders caused by stroke, spinal cord injury, traumatic brain injury, and deterioration of limb function is increasing^[1]. Patients



© The Author(s) 2024. **Open Access** This article is licensed under a Creative Commons Attribution 4.0 International License (<https://creativecommons.org/licenses/by/4.0/>), which permits unrestricted use, sharing, adaptation, distribution and reproduction in any medium or format, for any purpose, even commercially, as long as you give appropriate credit to the original author(s) and the source, provide a link to the Creative Commons license, and indicate if changes were made.



with movement disorders are prone to complications such as muscle wasting, vascular stenosis, and decreased cardiopulmonary function without the proper rehabilitation training for a long period. To avoid complications and benefit motor function recovery, such patients need to undergo exercise rehabilitation after acute phase management such as clinical surgery and medication to restore limb motor function and improve self-care ability^[2]. Relevant medical literature shows that with early detection and scientific treatment of patients with movement disorders and limb rehabilitation training, the human nervous system can repair and reconstruct the damaged nerves^[3], and there would be a high probability of recovery for patients with mild symptoms, and basic daily life functions can be realised for patients with more severe symptoms. Therefore, rehabilitation training plays a crucial role in the recovery of patients with movement disorders. Traditional clinical rehabilitation training usually requires professional therapists to provide individual or group rehabilitation guidance to patients^[4]. However, in China, rehabilitation remains in the initial development stage, facing challenges such as the majority of patients needing rehabilitation, a long training cycle for physicians, and a shortage of professional rehabilitation practitioners.

Therefore, rehabilitation robots have become a research hotspot in the field of robotics^[5]. They can not only reduce the physical burden of therapists but also save medical resources and reduce the cost of rehabilitation training. Their advantages over traditional manual training methods include: (a) They have the advantage of repeated training over a long period; (b) The robot-assisted rehabilitation can ensure the consistency of postural accuracy and intensity of each training session; (c) They have the freedom of time for rehabilitation training without the influence of manual trainers; (d) The convenience of data recording only requires the rehabilitation physiotherapist to give training advice on data testing, reducing the cost of hiring a long-term rehabilitation physiotherapist. It can be seen that robotic rehabilitation training has obvious advantages over traditional manual rehabilitation training. The research on rehabilitation robots is of great academic and practical significance.

This study focuses on the current development status of upper limb rehabilitation robots, which can be classified into two categories based on their mechanical structure: end-effector-based and exoskeleton-based^[4]. Representative examples of end-effector-based robots include MIT-Mannus^[6], Mirror Image Motion Enabler (MIME)^[7,8], GENTLE/s^[9], and others. This structural type cannot independently drive individual joints of the upper limb. In contrast, exoskeleton-based robots mimic the physiological structure of the human limbs, with joint layouts corresponding to those of the human body. Consequently, they can simultaneously guide coordinated movements of various joints^[10]. Robots, such as ARMin^[11,12], Harmony^[13], “u-Rob”^[14], and RUPERT^[15], fall into the category of exoskeleton robots. Rehabilitation training can be broadly divided into passive and active training stages. In the passive training process, the robot takes an active role in executing movements, and the patient is in a passive state, allowing the robot to guide the affected limb through corresponding training actions to achieve rehabilitation goals^[16]. However, this training process is limited to patients without muscle strength. Continuous passive training methods do not significantly improve the limb motor function of patients. Utilising robots as assistants to actively involve patients in rehabilitation training proves to be a more effective rehabilitation approach^[17]. Active training emphasises the rehabilitation robot following the movement intent of a patient through corresponding assistive control, where the patient takes the lead, thereby more effectively eliciting spontaneous participation in rehabilitation training^[18]. Due to the substantial joint reduction ratio and the lack of the ability for reverse driving in exoskeleton robots, patients cannot alter the robot motion trajectory using their own strength^[19]. Therefore, achieving assistive control of exoskeleton robots in an active training mode becomes a challenging problem^[13].

Rehabilitation robots prioritize the estimation of continuous control motion intent in active rehabilitation training. This method can be broadly categorised into three types: the interaction force-based, the electromyographic (EMG) signal-based, and the desired trajectory-based methods. The interaction force-based motion intent estimation method combines force/torque sensors with impedance control. It measures interaction

forces using external joint torque sensors or end-effector six-dimensional sensors to identify the motion intent and subsequently conduct active rehabilitation training. Kim *et al.* used force sensors to obtain interaction forces^[20], while Radke *et al.* employed a nonlinear disturbance observer based on a dynamic model to estimate interaction forces^[21]. The estimation of EMG signal-based motion intent involves establishing the relationship between EMG signals and muscle forces using the Hill muscle model, combined with a skeletal model, to calculate joint torques. Rosen *et al.* implemented this method's control on a two-axis robot^[22]. Hashemi and Ison, on the other hand, directly established the mapping relationship between EMG signals and joint torques using deep learning approaches^[23,24]. The desired trajectory-based motion intent estimation acquires the expected trajectory of a robot through interaction information and tracks it. Khan *et al.* used neural networks to establish a mathematical model between interaction information and the desired trajectory, achieving human-robot cooperative control^[25]. In terms of active motion intent recognition, due to the inconsistency and susceptibility of EMG signals to external factors such as electrode position, sweat, and humidity, the desired trajectory method requires constructing a complex expected trajectory model. Therefore, this paper adopts the interaction force-based motion intent estimation method, installing joint torque sensors at the joints to detect human-robot interaction forces without additional devices.

Zero-force control is the foundation for implementing active training, and traditional zero-force control primarily includes two methods: position control-based and torque control-based. In position control-based zero-force control, the robot operates in position control mode, leveraging external sensors as feedback units for force information. This method allows for precise detection of external force magnitude, providing higher sensitivity and stability. Direct teleoperation functionality is achieved by tracking position information, and external force detection requires external sensors or conversion through joint current values. Precise calculation of the dynamic model is needed, and the method demands high sensor accuracy but exhibits poor robustness^[26,27]. In torque control-based zero-force control, the robot operates in torque control mode, eliminating external sensors and only requiring compensation for gravity and friction in the dynamic model^[28,29]. However, challenges arise in overcoming inertial forces, motor internal reducer transmission losses, and other uncertainties during motion. For patients with movement disorders, especially those with weak muscle strength, overcoming the robot's inertial forces and other impediments for rehabilitation training is challenging. Therefore, this method falls short of meeting the requirements for active training. The precision of dynamic model parameter identification is compromised due to uncertainties such as friction and internal motor reducer transmission losses^[30].

In this paper, firstly, under the zero force control of the robot, a form based on the combination of outer-loop PID feedback and feedforward control is proposed. The robot works in the torque control mode, calculates the interaction force by computing the dynamics model using external torque sensors, and obtains the compensation value of the feedforward torque by means of the outer-loop control, which not only provides the compensation torque of the external force but also overcomes the inaccuracy of the dynamics model and improves the robustness of the system. Meanwhile, an active rehabilitation training method based on outer-loop fuzzy PID control is further proposed to address the shortcomings of ordinary PID control. The traditional PID method has limitations in compensating torque with fixed parameters, which may not be suitable for all patients, particularly those at different stages of rehabilitation treatment. Fuzzy PID control is more suitable for the active rehabilitation training function compared to the normal PID control method^[31]. First, it is more robust to system nonlinearity and uncertainty and can better overcome the influence of uncertainty factors in the dynamics model. Secondly, it is more responsive to the system and can respond faster to the motor intention of a patient^[32], which, in turn, enables the patient to provide less interaction force to complete the active rehabilitation training and improves the rapidity and suppleness of the system.

This paper is organised as follows. Section 2 describes the rehabilitation robot device and modelling method. Section 3 presents the active training method based on outer-loop PID and its fuzzy control improvement

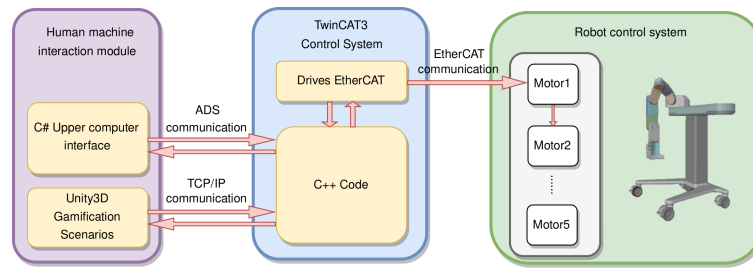


Figure 1. Block diagram of robot system operation.

algorithm. Section 4 gives the results of the validation experiments. Section 5 designs a gamified scenario-based active rehabilitation training scheme based on the improved algorithm, and finally, Section 6 gives the conclusions of this paper and the direction of future work.

2. ROBOTIC DEVICE MODELLING

Upper-limb rehabilitation robots are divided into two categories: end-traction and exoskeleton^[33]. End-pull robots interact with the hand or arm of a patient through an end-effector to drive other upper limb joints to move. The exoskeleton robot imitates the human physiological structure, and the joint distribution corresponds to the human joints, which can guide the movement of all human joints at the same time and provide comprehensive joint movement information and targeted training^[10].

Therefore, we developed a 5-degree-of-freedom exoskeleton robot, in which the shoulder is represented by three articulated motor couplings, and the elbow and wrist are each controlled by a single motor. Each motor joint is equipped with a joint torque sensor, where the large arm linkage and the small arm linkage are set as adjustable structures in order to adapt to the arm length of the patient. The shoulder joints of upper limb exoskeletons are usually represented by three vertically aligned rotary joints. In order to enhance the range of motion while avoiding mechanical singularities and interference with the human body, our shoulder joint consists of three rotary joints aligned at an acute angle, and the angles between the axes are set as 60 degrees.

The robot hardware device adopts an industrial computer as the robot control system operation platform, and the motor controller is connected to the industrial computer through the EtherCAT bus protocol, which has better clock synchronisation than the common Ethernet connection technology. In terms of software, TwinCAT3 software is used, running on the industrial control machine. At the same time, CSharp upper computer interaction software is developed to achieve data transfer through ADS communication; Unity3D gamification scene technology is developed to achieve synchronisation of movements through TCP/IP communication. The above hardware selection and data interaction methods constitute the control system of this robot. The block diagram of the robot system operation is shown in [Figure 1](#). The robot is modelled, and the structure is shown in [Figure 2](#).

A Modified Denavit-Hartenberg (MDH) parameter construction method is used to build the MDH parameter table [[Table 1](#)]. α_{i-1} , a_{i-1} , d_i , and θ_i denote the connecting rod torsion angle, connecting rod length, joint angle, and joint offset, respectively. Row s of the table represents the transformation relationship from the base coordinate to the 0 coordinate system. The units of a_i and d_i are in millimetres.

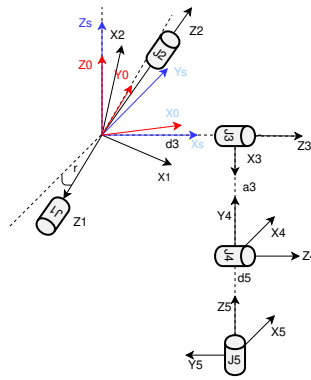


Figure 2. Robot model.

Table 1. MDH parameters

i	α_i	a_i	d_i	θ_i
s	0	0	0	30
1	90	0	0	$\theta_1 - 19.14712$
2	-60	0	0	$\theta_2 + 70.5288$
3	60	0	102.74	$\theta_3 - 109.4712$
4	0	270	0	$\theta_4 + 90$
5	-90	0	-195	θ_5

MDH: Modified Denavit-Hartenberg.

2.1 Kinematic analysis

According to the parameter table, the coordinate transformation relationship between the joints can be expressed in the form of a rotation matrix and a position matrix; the rotation matrix is given as

$${}^sR = Z_\gamma X_{\alpha_0} Z_{\theta_1} X_{\alpha_1} Z_{\theta_2} X_{\alpha_2} Z_{\theta_3} Z_{\theta_4} X_{\alpha_4} Z_{\theta_5} \tag{1}$$

and the position absolute matrix is defined as

$${}^sP = Z_\gamma X_{\alpha_0} Z_{\theta_1} X_{\alpha_1} Z_{\theta_2} \begin{bmatrix} 0 \\ -s\alpha_2 d_3 \\ c\alpha_2 d_3 \end{bmatrix} + Z_\gamma X_{\alpha_0} Z_{\theta_1} X_{\alpha_1} Z_{\theta_2} X_{\alpha_2} Z_{\theta_3} \begin{bmatrix} a_3 \\ 0 \\ 0 \end{bmatrix} + Z_\gamma X_{\alpha_0} Z_{\theta_1} X_{\alpha_1} Z_{\theta_2} X_{\alpha_2} Z_{\theta_3} Z_{\theta_4} \begin{bmatrix} 0 \\ d_5 \\ 0 \end{bmatrix} \tag{2}$$

The derivation and transformation of the forward and inverse kinematics of a robot can be achieved through the rotation and position matrices, realising the mutual mapping between the exoskeleton robot’s joint space and under the Cartesian space. Through the forward and inverse kinematics resolution, it completes the execution of the trained motion along the pre-set desired trajectory, for example, shoulder joint adduction and abduction, forward and backward flexion and extension, internal and external rotation movements, elbow flexion and extension movements, and wrist turning movements. In the passive training mode, the purpose of the robot controller is to reduce the trajectory tracking error, so that the patient learns the correct movement pattern, usually in the form of traditional closed-loop control combined with feedforward compensation.

2.2 Identification of dynamical model parameters

Whether it is the feedforward compensation function in passive training or the interactive force-assisted control function in active training, it is necessary to establish the kinetic model of the rehabilitation robot to calculate the moment information in the motion state, and this paper adopts the method of kinetic identification to obtain the kinetic parameters of the robot and complete the construction of the model. Because the

fifth joint of the robot device has a lightweight mechanical structure and works in the moment mode with almost zero resistance, the kinetic model is not established for this joint, and this operation can reduce the complexity of the robot model and improve the model accuracy. Therefore, the dynamics model of this robot is a 4-degree-of-freedom model.

2.2.1 Kinetic model construction

The Newton-Euler method is used to build a dynamics model for this robot. Compared with the Lagrangian modelling method, this approach calculates through the inter-joint force and motion relationship layer by layer, the physical meaning is clear, and it does not involve derivation operation, so that the results can be obtained quickly and the calculation efficiency is high [34]. The standard form of its expression is given as

$$\tau = M(q)\ddot{q} + H(q, \dot{q}) + G(q) + \xi(q, \dot{q}, \ddot{q}) \quad (3)$$

where q, \dot{q}, \ddot{q} represent the position, velocity and acceleration vectors of the joint, respectively, τ denotes the joint torque vector, $M(q)$ is the mass matrix, $H(q, \dot{q})$ is the centrifugal and Koch force vectors, $G(q)$ denotes the gravitational moment, and $\xi(q, \dot{q}, \ddot{q})$ denotes the other compensating moment parameters.

2.2.2 Linearisation of the model

The kinetic parameters of the robot are represented in the kinetic model in a nonlinear combination, which makes it difficult to identify the kinetic parameters. Through the parallel axis theorem, the coordinate system of the inertial parameter in the nonlinear term is coordinate transformed to complete the linearisation process [35]. The force and moment expressions in the kinetic model are given in

$$\begin{aligned} {}^i f_i &= {}_{i+1}^i R^{i+1} f_{i+1} + m_i {}^i \dot{\omega}_i \times {}^i P_{C_i} + m_i {}^i \omega_i \times ({}^i w_i \times {}^i P_{C_i}) + m_i {}^i \dot{v}_i \\ {}^i n_i &= {}_{i+1}^i R^{i+1} n_{i+1} + {}^i P_{i+1} \times {}_{i+1}^i R^{i+1} f_{i+1} + {}^i P_{C_i} \times m_i {}^i \dot{v}_i + {}^i \omega_i \times {}^i I_i {}^i \omega_i + {}^i I_i {}^i \dot{\omega}_i \end{aligned} \quad (4)$$

where f, n are the force and moment on the articulated linkage, ${}_{i+1}^i R$ is the coordinate transformation matrix, $\dot{v}, \omega, \dot{\omega}$ represents the linear acceleration, angular velocity, and angular acceleration of the articulated linkage of the rehabilitation robot, respectively, ${}^i P_{i+1}$ is the vector from the origin of the coordinate system of the i th articulated linkage (i.e., the i coordinate system) to the origin of the coordinate system of the $i+1$ th articulated linkage, m is the mass of the articulated linkage, and ${}^i P_{C_i}$ represents the centre of mass of the articulated linkage. I denotes the inertia tensor matrix. The identification equation for the kinetic parameters can be expressed as:

$$\tau_s = H(q, \dot{q}, \ddot{q})\theta \quad (5)$$

where $H(q, \dot{q}, \ddot{q}) \in R^{m \times n}$ denotes the observation matrix; m and n denote the number of kinetic parameters in the kinetic parameter set and the number of robot rods, respectively. $\theta \in R^{m \times 1}$ is the set of dynamics parameters. Since some columns of $H(q, \dot{q}, \ddot{q})$ are always zero and some columns have a linear relationship, no matter what value of q, \dot{q}, \ddot{q} is taken, H cannot make the columns full rank, and thus θ cannot be solved uniquely by the least-squares method. In this section, we use the QR decomposition method. The matrix H is decomposed to full rank, and the result of the decomposition is used to restructure the inertia parameters. The following formula can be obtained:

$$\tau = \tilde{H} P_{Base} \quad (6)$$

where \tilde{H} is the matrix of column full-rank coefficients obtained from the full-rank decomposition of H . P_{Base} is the minimum inertia parameter after reorganisation.

2.2.3 Fourier excitation trajectory

In the realm of robot dynamics parameter identification, the judicious linearisation of the model ensures the unique convergence of identification results toward the target values. Discrepancies between target and true values primarily stem from kinematic parameter deviations and measurement noise. Rational design of identification excitation trajectories serves to mitigate the impact of measurement noise on results and enhance

the iterative speed of target parameter convergence, thereby elevating identification accuracy. Atkeson *et al.* employed a fifth-degree polynomial method as the excitation trajectory in joint space^[36]. However, due to the coupled relationship between joints in the joint space of the rehabilitation robot investigated in this study, this method is not suitable. Swevers introduced, for the first time, an excitation trajectory model based on Fourier series^[37]. This trajectory possesses periodicity, smoothness, and strong robustness, making it widely applicable in future research. Therefore, this paper adopts the Fourier series method for obtaining the excitation trajectory, optimising the trajectory parameters based on the matrix condition number, and ultimately obtaining a relatively ideal excitation trajectory. The signal-to-noise ratio of the data is improved by averaging through multiple samples, enhancing data quality. The overdetermined equations used in the parameter identification process for a periodic excitation trajectory model composed of a finite number of Fourier series terms are formulated, as given in

$$\mathbf{T} = \begin{bmatrix} \tau(t_1) \\ \tau(t_2) \\ \vdots \\ \tau(t_N) \end{bmatrix} = \begin{bmatrix} H_M(\mathbf{q}(t_1), \dot{\mathbf{q}}(t_1), \ddot{\mathbf{q}}(t_1))_{n \times N_b} \\ H_M(\mathbf{q}(t_2), \dot{\mathbf{q}}(t_2), \ddot{\mathbf{q}}(t_2))_{n \times N_b} \\ \vdots \\ H_M(\mathbf{q}(t_N), \dot{\mathbf{q}}(t_N), \ddot{\mathbf{q}}(t_N))_{n \times N_b} \end{bmatrix} \mathbf{X}_{\min} = \mathbf{H}_\tau \mathbf{X}_{\min} \tag{7}$$

where H_M represents the regression matrix, X_{\min} denotes the minimum parameter set to be identified, and H_τ corresponds to the vector of filtered torque sampling data. The form of the excitation trajectory is specified as per

$$q_i(t) = q_{i0} + \sum_{n=1}^N \frac{a_{in}}{n\omega_f} \sin(n\omega_f t) - \frac{b_{in}}{n\omega_f} \cos(n\omega_f t) \tag{8}$$

where q_{i0}, a_{in}, b_{in} represent the coefficients of the fitted trajectory, ω_f is the fundamental frequency of the Fourier series, N is the order, and excitation trajectory of each joint comprises $(2N + 1)$ parameters. This study adopts a 5th-order Fourier series, with 11 parameters needing determination for the excitation trajectory of each individual joint during a single run. The specific constraints on the trajectory are outlined in

$$\begin{cases} |q_i(t)| \leq q_{\max} & \forall i, t \\ |\dot{q}_i(t)| \leq v_{\max} & \forall i, t \\ |\ddot{q}_i(t)| \leq a_{\max} & \forall i, t \\ q_i(t_0) = q_i(t_f) = 0 & \forall i, t \\ \dot{q}_i(t_0) = \dot{q}_i(t_f) = 0 & \forall i, t \\ \ddot{q}_i(t_0) = \ddot{q}_i(t_f) = 0 & \forall i, t \end{cases} \tag{9}$$

where A denotes the maximum values of the angle, angular velocity, and angular acceleration for each joint, with the equality conditions ensuring that the states at the start and end times of the trajectory period are both 0. For the optimisation function design problem of such excitation trajectory models, the quality of the excitation trajectory is related to the ill-conditioning of the observation matrix. Therefore, optimising the excitation trajectory is achieved by using the condition number of the observation matrix as the criterion. A smaller condition number is favourable, as it reduces the susceptibility to the impact of errors introduced by self-noise when solving parameters using the least squares method. The condition number is given as

$$cond(\psi) = \frac{\sigma_{\max}(\psi)}{\sigma_{\min}(\psi)} \tag{10}$$

Here, $\sigma_{\max}(\psi)$ and $\sigma_{\min}(\psi)$ respectively represent the maximum and minimum singular values of the matrix ψ . The objective function for optimising the excitation trajectory parameters is to minimise the condition number of the regression matrix in the dynamic model. As a multi-constraint nonlinear optimisation problem, the trajectory is optimised using the `fmincon` function in the MATLAB optimisation toolbox, solving for the 44 parameters in the excitation trajectory. The excitation trajectory plot is illustrated in [Figure 3](#).

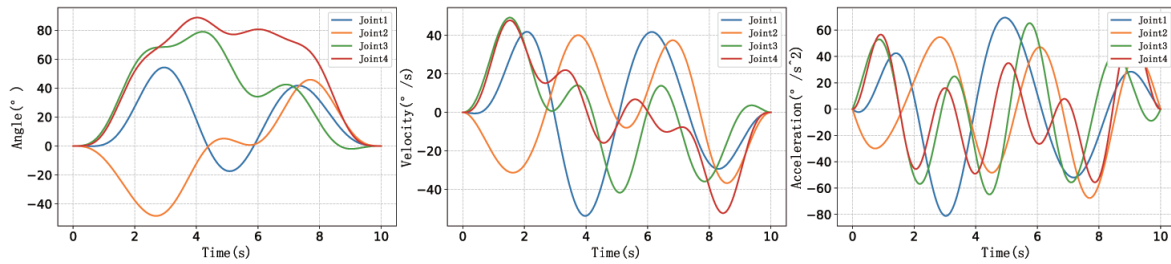


Figure 3. Incentive trajectory motion curve.

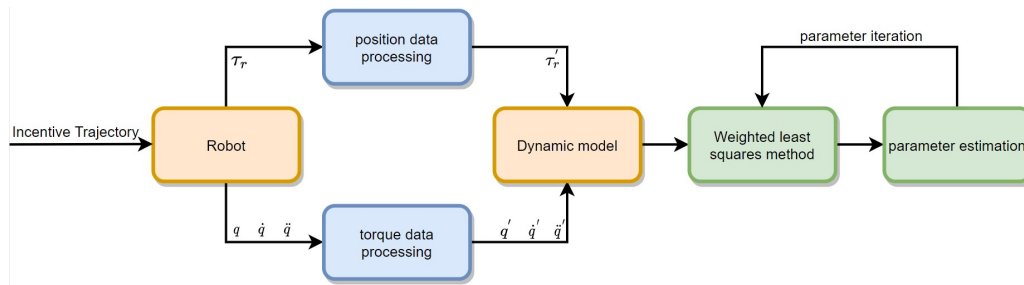


Figure 4. Identification flow chart.

According to the motion curves in Figure 3, it can be seen that the excitation trajectory of the robot meets the optimisation conditions of the objective function, and the condition number of the regression matrix after the convergence of the objective function is $88.78 < 100$. This is consistent with the results of the related experiments of this category at national and international standards.

2.2.4 Parameter identification and validation

In accordance with the weighted least squares method, the solution under the minimum parameter set is obtained, as given in

$$X_{WLS} = \left(H^T \Sigma^{-1} H \right)^{-1} H^T \Sigma^{-1} \Gamma \tag{11}$$

where Σ^{-1} represents the covariance matrix of the torque measurement value noise standard deviation, H is the observation matrix, Γ is the torque measurement value vector, and X_{WLS} is the identification vector. The identification process for the robotic dynamic parameters in the context of rehabilitative robotics is illustrated in Figure 4. The identification model of the robot is determined by the minimum parameter set and the corresponding regression matrix, while the input positions of the robot control law are dictated by the excitation trajectory. Due to the real-time nature of motion data, a first-order low-pass filter is applied to filter the motion data. Ultimately, the identification results based on a fifth-order Fourier series excitation trajectory are presented in Figure 5. The figure illustrates the mathematical dynamic model predicting torque for the identification trajectory, with the predicted torque (depicted by the solid orange line), actual torque (depicted by the solid blue line), and the error between the two (depicted by the solid green line). It is evident from the figure that the computed torque values closely follow the trend of the actual values, confirming the accuracy of the identification model. The overall assessment of the accuracy of the identification results is determined through the Root Mean Square Error (RMSE) and Mean Absolute Error (MAE) metrics [Table 2]. The RMSE is defined as

$$RMSE = \sqrt{\frac{\sum_{i=1}^{n_{total}} (X_{i, calc} - X_{i, act})^2}{n_{total}}} \tag{12}$$

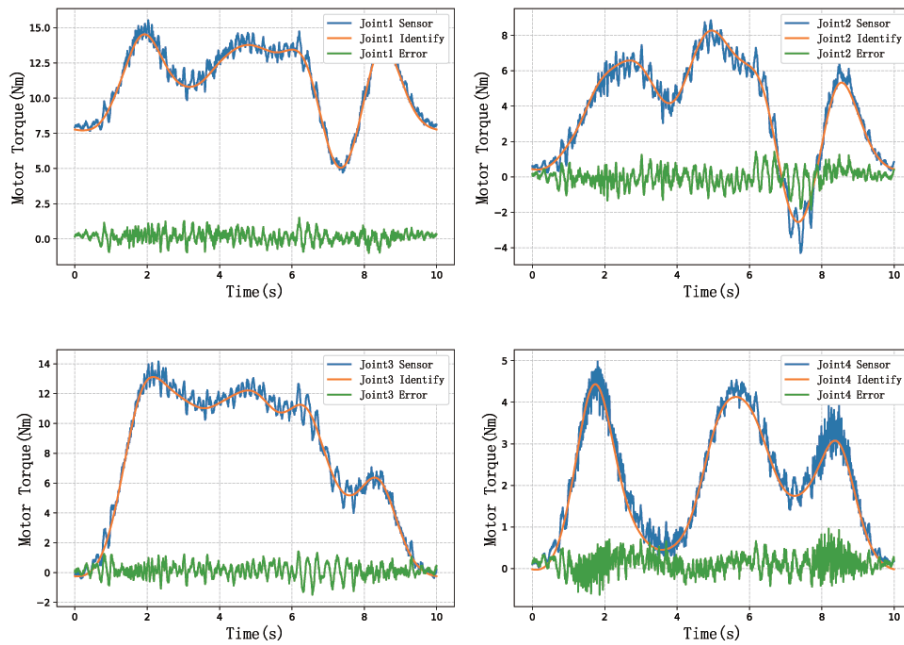


Figure 5. Parameter identification result diagram.

Table 2. Parameters of RMSE/MAE indicators table

	Joint1	Joint2	Joint3	Joint4
RMSE	0.422	0.492	0.469	0.246
MAE	0.335	0.377	0.364	0.198

RMSE: Root Mean Square Error; MAE: Mean Absolute Error.

where n_{total} represents the number of data points, and $X_{i, calc}, X_{i, act}$ denote the calculated and actual values for the $i - th$ data point, respectively. The MAE is defined as:

$$MAE = \frac{1}{N} \sum_{i=1}^N |\hat{\tau}_i - \tau_i| \tag{13}$$

where $\hat{\tau}_i$ represents the actual observed values, τ_i represents the predicted values, and N represents the number of samples.

Upon computation, the overall RMSE for the joint identification results is calculated to be 1.629 Nm, with an overall MAE of 1.274 Nm and a torque average error rate of 6.65%. These results align with the identification requirements.

In the context of robot dynamics parameter identification, parameter validation stands as an indispensable step. It not only scrutinises the entire identification process for potential errors but also ensures the accuracy of the obtained dynamic parameters, laying a foundation for subsequent active rehabilitation training. In this study, a third-order Fourier series trajectory model is employed to generate a new trajectory distinct from the identification process. This trajectory ensures that the validation trajectory is entirely different from the excitation trajectory during parameter identification and exhibits as substantial motion as possible. Its results using the third-order Fourier series are illustrated in Figure 6.

As shown in the figure above, after the validation of the parameter identification by using the new excitation trajectory, the relative error of the moment of the validated trajectory is 7.62%, and this validation method

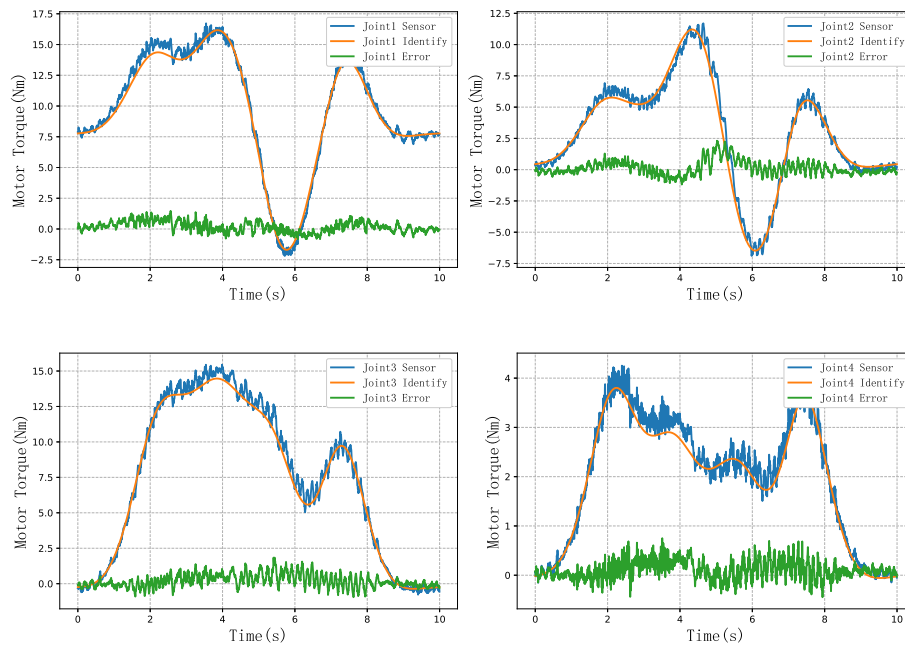


Figure 6. Joint identification verification results.

proves the high accuracy of the identified parameter values and the good moment prediction effect when applied to the robot dynamics.

3. ACTIVE TRAINING METHOD BASED ON OUTER LOOP PID

The ideal state for assistive control in exoskeleton robots is to enable the motion of an operator without interference from the robot, commonly referred to as "transparent" control [38,39]. In this study, torque sensors are integrated at the joints of the rehabilitative robot, allowing real-time monitoring of the torque exerted by the robot. This facilitates the extraction of human-robot interaction forces, subsequently serving as input for the controller to execute the assistive control of the exoskeleton robot.

In traditional zero-force control, precision dynamic models are required for position-based zero-force control, imposing high demands on sensor accuracy and exhibiting poor robustness. In torque-based zero-force control, although external sensors are not needed, and only gravity and friction compensation are required, uncertainties such as inertial forces and motor transmission losses prevent it from meeting the requirements of active training.

To address the shortcomings of traditional zero-force control methods in active rehabilitation training, a strategy based on outer-loop PID control is proposed, incorporating joint torque sensors at the robot joints. This approach utilises external sensors to calculate interaction forces, obtaining compensation values for feedforward torque through outer-loop control. This not only provides compensation torque for external forces but also enhances the robustness of robots to inaccuracies in the dynamic model. Through this control method, the smoothness of the active rehabilitation training process can be improved.

Although traditional outer-loop PID algorithms address the issue of insufficient torque output from the dynamic model, they exhibit limitations in compensating for torque due to fixed parameters. This approach may not be universally suitable for all patients, especially those in different stages of rehabilitation treatment.

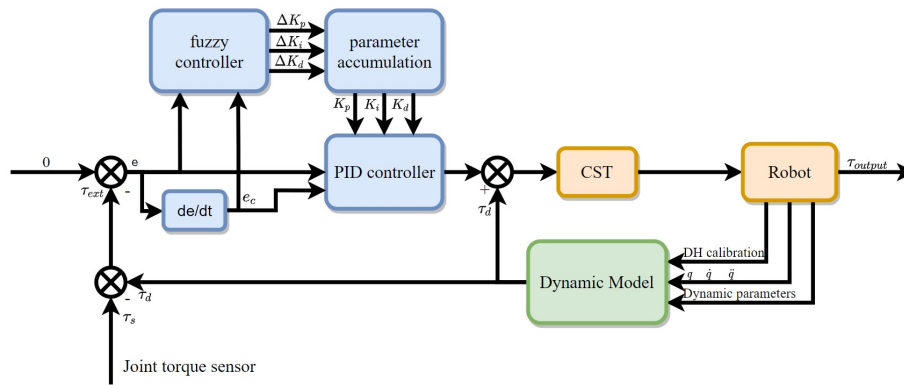


Figure 7. Improved control structure diagram.

Fuzzy PID control presents significant advantages in two aspects: firstly, it demonstrates enhanced robustness, effectively handling system nonlinearity and uncertainties to overcome uncertainties in the dynamic model. Secondly, it results in a faster system response, enabling a quicker capture of the motion intent of a patient. Consequently, patients can accomplish active rehabilitation training with reduced interaction forces, enhancing the responsiveness and flexibility of systems. The improved network structure diagram using the fuzzy control algorithm is illustrated in Figure 7. The joint actuators of the system operate in torque mode, and the control system expression is given as

$$\tau_d(t) = K_p \cdot e(t) + K_d \cdot (e(t) - e(t - 1)) + \tau_c(t) \tag{14}$$

$$e(t) = \tau_{ext}(t) - 0 \tag{15}$$

$$\tau_{ext}(t) = \tau_s(t) - \tau_d(t) \tag{16}$$

Fuzzy control is a novel intelligent control method based on fuzzy set theory, linguistic variables, and logic reasoning. Its essence lies in utilising expert experience to simulate human behaviour for decision-making and control [40]. Here, e represents the input error, and ec represents the error change rate. Fuzzy rehabilitation robot interaction force input error and error change rate are fuzzified to obtain the fuzzy subset E, EC . Through fuzzy relations and logical reasoning, the output set $\{\Delta k_p, \Delta k_i, \Delta k_d\}$ is derived. The output is then defuzzified to transform it into precise values $\{\Delta k_p, \Delta k_i, \Delta k_d\}$ which are added to the conventional PID parameters. Finally, the values of k_p, k_i and k_d are obtained and transmitted to the robot joints, realising active rehabilitation training for the robot.

In this control framework, the traditional outer-loop PID control is used as the basis of this paper’s framework, and the outer-loop PID control is improved with fuzzy algorithms so that the parameters in the PID control are variable. The errors of human-robot interaction force and zero-target torque are taken as inputs, processed through the fuzzy PID controller to calculate the required compensation force. This compensation force is then added to the torque calculated by the dynamic model, enabling the robot system to operate in torque mode. This process achieves torque compensation and facilitates the active rehabilitation training.

The entire process of the fuzzy control algorithm consists of four stages: fuzzification of input and output variables, design of fuzzy control rules, logical inference, and defuzzification, to achieve precise control of the rehabilitation robot. The fuzzy control input variables include $\{E, EC\}$, and the output variables include $\{\Delta k_p, \Delta k_i, \Delta k_d\}$. Fuzzy subsets are defined as $[NB, NM, NS, ZO, PS, PM, PB]$, representing large negative, medium negative, small negative, zero, small positive, medium positive, and large positive. The membership table for input and output variables is obtained through triangular membership functions. In this paper, the fuzzy control is applied to PID parameter correction. In accordance with previous experimental experiences, the derived inference rules are presented in Tables 3-5.

Table 3. *e, ec, Δkp* affiliation table

Output	EC						
E	PB	PB	PM	PM	PS	ZO	ZO
	PB	PB	PM	PS	PS	ZO	NS
	PM	PM	PM	PS	ZO	NS	NS
	PM	PM	PS	ZO	NS	NM	NM
	PS	PS	ZO	NS	NS	NM	NM
	PS	ZO	NS	NM	NM	NM	NB
	ZO	ZO	NM	NM	NM	NB	NB

Table 4. *e, ec, Δki* affiliation table

Output	EC						
E	PB	PB	PM	PM	PS	ZO	ZO
	PB	PB	PM	PS	PS	ZO	NS
	PM	PM	PM	PS	ZO	NS	NS
	PM	PM	PS	ZO	NS	NM	NM
	PS	PS	ZO	NS	NS	NM	NM
	PS	ZO	NS	NM	NM	NM	NB
	ZO	ZO	NM	NM	NM	NB	NB

Table 5. *e, ec, Δkd* affiliation table

Output	EC						
E	PB	PB	PM	PM	PS	ZO	ZO
	PB	PB	PM	PS	PS	ZO	NS
	PM	PM	PM	PS	ZO	NS	NS
	PM	PM	PS	ZO	NS	NM	NM
	PS	PS	ZO	NS	NS	NM	NM
	PS	ZO	NS	NM	NM	NM	NB
	ZO	ZO	NM	NM	NM	NB	NB

Its trigonometric affiliation function is defined as

$$f(x; a, b, c) = \left\{ \begin{array}{ll} 0, & x \leq a \\ \frac{x-a}{b-a} & a \leq x \leq b \\ \frac{c-x}{c-b} & b \leq x \leq c \\ 0, & c \leq x \end{array} \right\} \tag{17}$$

Fuzzy inference involves deriving new conclusions based on existing fuzzy conditions or assumptions, with the Mamdani inference method being a commonly used approach. The algorithm involves a direct product operation for fuzzy implications $Q_{ij}(E, EC, \Delta M)$ as a fuzzy set E'_i, EC'_j, M'_{ij} , based on the minimum constraint relation. Here, E represents the error, EC is the error change rate, and M is an adjustment value. The specific algorithm involves direct product operations, where $i = 1 \dots 7, j = 1 \dots 7$ represent fuzzy set linguistic values, expressed as

$$Q_{ij}(E, EC, \Delta M) \in E'_i \times EC'_j \times \Delta M'_{ij} \tag{18}$$

For a discrete domain fuzzy set $E'_i, EC'_j, \Delta K'_{pij}$ represented as a matrix, it can be expressed as

$$D_{ij}(E, EC) = E'_i \times EC'_j = E'^T_i \wedge EC'_j \tag{19}$$

$$Q_{ij}(E, EC, \Delta M) = D_{ij}(E, EC) \wedge M'_{ij} \tag{20}$$

where $D_{ij}(E, EC)$ represents the transformation of the first-row elements into columns, and subsequent rows follow suit. If the controller has n fuzzy rules, the fuzzy relation Q is constructed from n fuzzy implication relations Q_{ij} , defined as

$$Q = \bigcup_{i=1, j=1}^{i=7, j=7} Q_{ij}(E, EC, \Delta M) \tag{21}$$

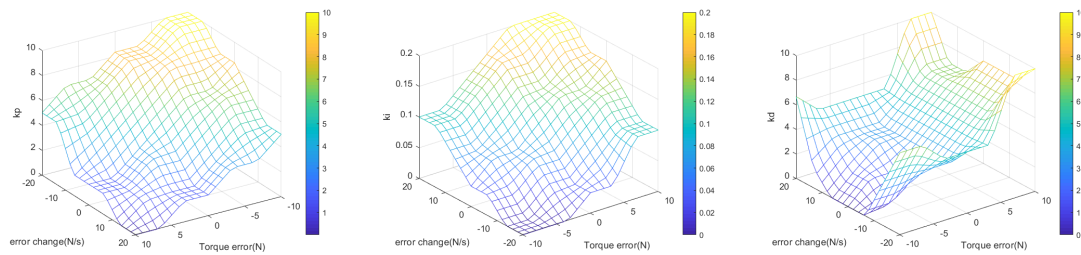


Figure 8. Fuzzy controller input-output relationship diagram.

By mapping e and ec to the corresponding control parameters k_p, k_i, k_d according to the fuzzy rule table, and subsequently applying defuzzification using the method of maximum membership, the fuzzy inference is refined. With k_p as an example, precise values in the form of $\{\Delta k_p, \Delta k_i, \Delta k_d\}$ are obtained, as illustrated by $k_p = \max f_M(\Delta k_p), \Delta k_p \subset M$.

In accordance with the practical considerations in rehabilitation, the adjustment magnitude of the interaction force in the conventional PID control method should not be excessively large, and the adjustment rate is typically set to a low value. Therefore, the proportional coefficients for the first three joints are set to 5. To enhance joint response speed and eliminate steady-state error, the integral coefficient is set to 0.1. Additionally, to suppress joint oscillations, the derivative coefficient is set to 5. Given the smaller mass of the fourth joint and its faster tracking response, the integral coefficient is set to 0. After incorporating a fuzzy controller into the PID control, during the parameter adjustment process, the maximum value of torque error is set to ± 10 N, and the maximum rate of its change is set to ± 20 N/s, based on the torque variation during joint operation. According to the fuzzy subset configuration, each breakpoint is set to $1/3$ of the maximum specified error. Subsequently, the membership values for each fuzzy interval are calculated using a triangular membership function. In summary, the input-output relationship of this fuzzy controller is shown in [Figure 8](#).

In accordance with the aforementioned reasoning process, the error between human-robot interaction force and the system's zero torque, along with the rate of change of interaction force error, serves as inputs to the fuzzy controller. The change in PID parameters, computed as output, is used to dynamically adjust the PID parameter values in real time during the active rehabilitation training process. This aims to accelerate the response speed of a system and enhance the rehabilitation flexibility.

4. EXPERIMENTAL VERIFICATION

Training was conducted using two active rehabilitation control methods: one based on the conventional external-loop PID algorithm and the other based on the external-loop fuzzy PID algorithm. Data from joint torque sensors and computed data from dynamic identification were recorded during the training process, as illustrated in [Figures 9-12](#). The data collected from the joint torque sensors were left unfiltered to ensure real-time accuracy.

In the active training process, the blue curve represents the torque data collected by the joint torque sensor, the orange curve represents the torque data calculated from dynamic model parameter identification, and the green curve represents the error between sensor torque data and calculated torque data, representing the additional interactive force provided by the patient. Simultaneously, the torque data curves of fuzzy control and conventional control at the torque direction transition are locally magnified. The local graph shows the proposed fuzzy PID control method in this paper effectively reduces the phenomenon of sudden changes when

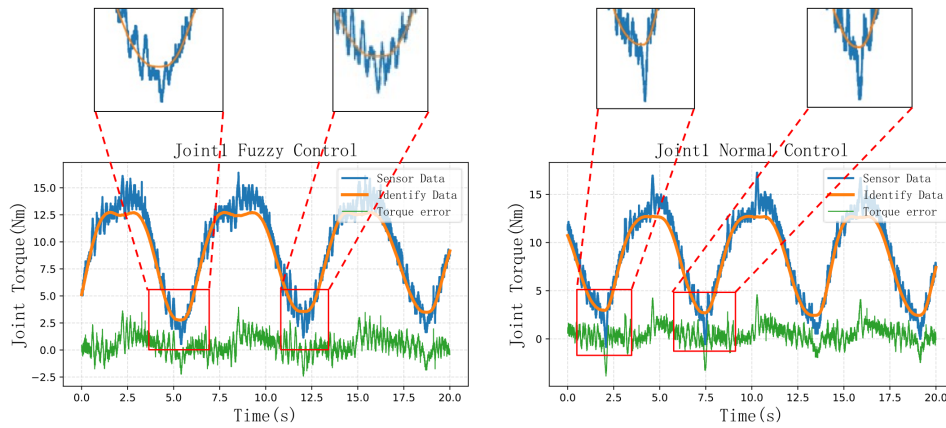


Figure 9. Comparison of joint1 torque data.

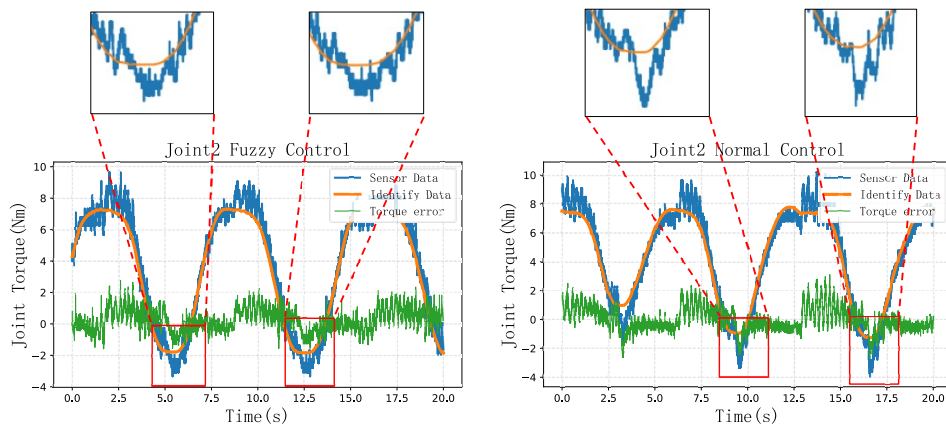


Figure 10. Comparison of joint2 torque data.

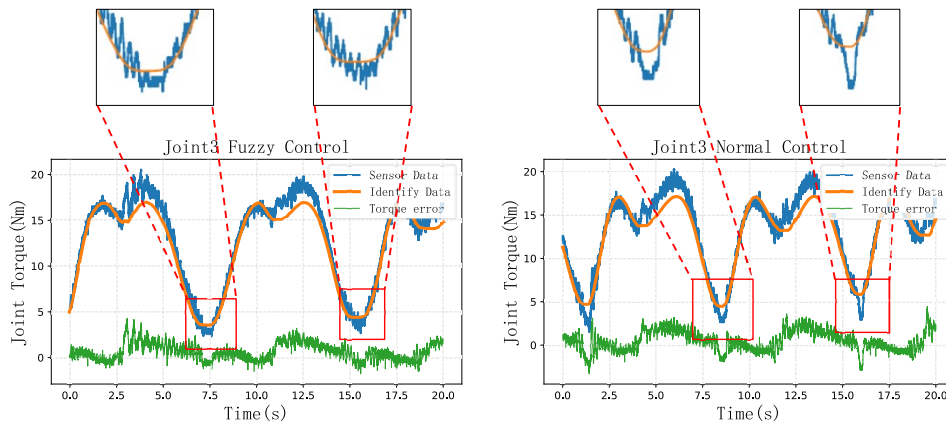


Figure 11. Comparison of joint3 torque data.

the torque changes direction. This is attributed to the stronger robustness of the fuzzy control method to system nonlinearity and uncertainty, resulting in faster system response. Additionally, the system can adaptively adjust PID parameters, enabling a quicker response to the motion intention of a patient, thereby allowing the patient to provide smaller interactive forces for active rehabilitation training. This enhances its agility and smoothness.

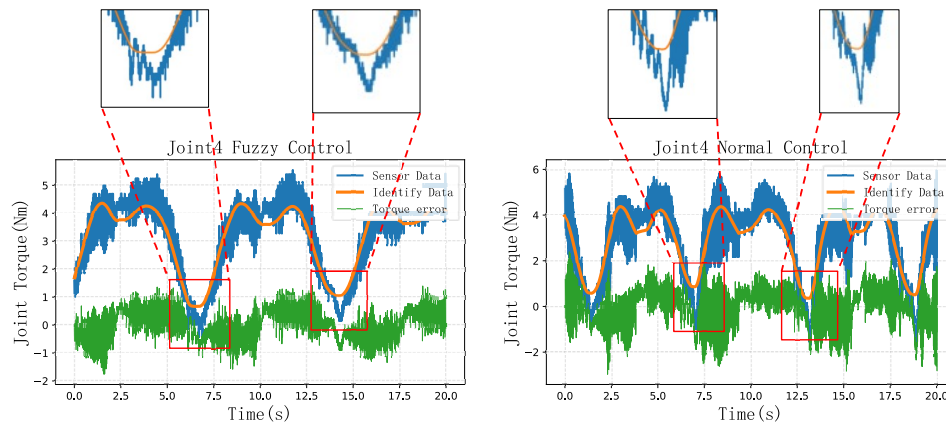


Figure 12. Comparison of joint4 torque data.

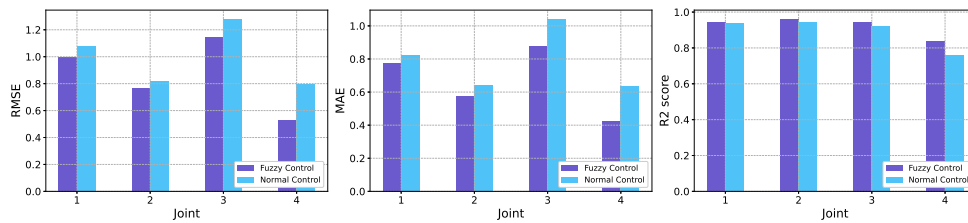


Figure 13. Comparison of *RMSE*, *MAE* and *R²* for normal and fuzzy control diagrams. *RMSE*: Root Mean Square Error; *MAE*: Mean Absolute Error.

Due to the fact that each action cycle in active rehabilitation training is genuinely captured by the patient, despite maintaining consistency in rehabilitative movements, it remains challenging to ensure complete uniformity in each instance of the action. Therefore, this paper conducts an overall experimental comparison of rehabilitative actions in active training based on fuzzy and conventional PID control. The evaluation of this experiment involves comparing and analyzing the results using three performance metrics: *RMSE*, *MAE*, and Coefficient of Determination (*R²*). The expression for the *R²* score is given as

$$R^2 = \frac{\sum_{i=1}^n (\hat{y}_i - \bar{y})^2}{\sum_{i=1}^n (y_i - \bar{y})^2} \tag{22}$$

where \hat{y}_i denotes the predicted value of the data, y_i represents the true value of the data, and \bar{y} stands for the average value of the data. The results of the experimental comparison are shown in [Figure 13](#).

As illustrated in the above figure, the purple and blue sections represent the *RMSE* and *MAE* evaluation metrics for torque data under fuzzy control and conventional control methods, respectively. It can be observed that the performance of the fuzzy control method for all four joints is superior to the conventional control method. The calculations indicate an average reduction of 15% in *RMSE* and *MAE* values for the four joints, accompanied by an average increase of 4% in coefficient of determination.

5. GAMIFICATION SCENARIO TRAINING PROGRAMME DESIGN

The emergence of rehabilitation robots has the potential to enhance rehabilitation efficiency, mitigate the impact of uncertainties associated with rehabilitation practitioners, and concurrently reduce costs. However, the

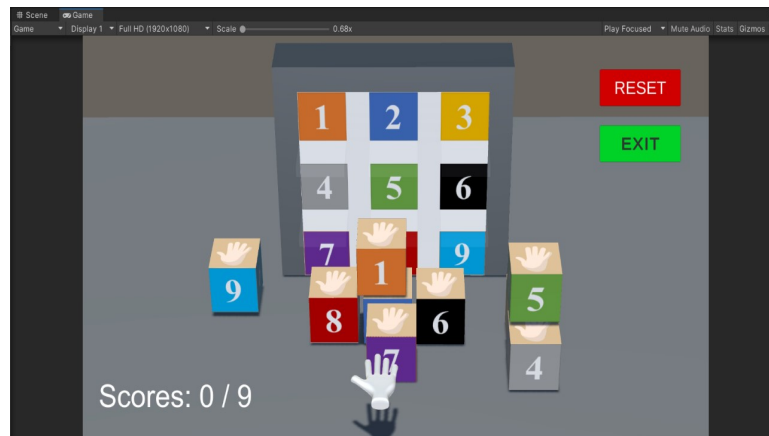


Figure 14. Gamification scenarios.

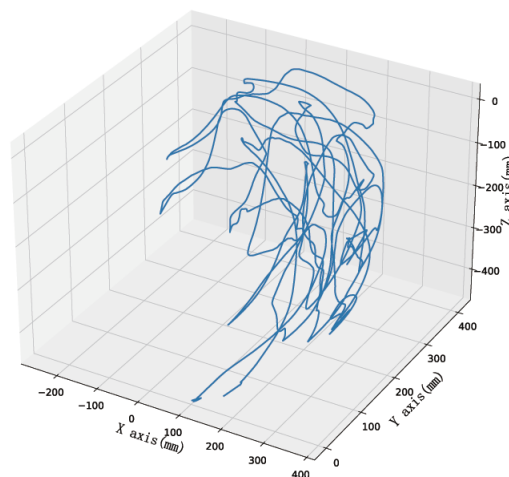


Figure 15. Virtual reality training 3D trajectory.

integration of robots does not necessarily address the drawbacks of prolonged and monotonous training cycles in the rehabilitation process. This monotony can lead to reduced patient motivation, thereby affecting the overall effectiveness of the training. The combination of virtual reality (VR) technology and robots offers a promising solution to boost rehabilitation motivation [41].

This paper presents the development of a wooden box placement game with visual feedback based on VR technology. The game involves arranging the wooden boxes on a numerical wall in correspondence with the numbers on each box. The rehabilitation robot operates in active training mode, allowing patients to actively engage in rehabilitation by manipulating the robot. During this process, the robot control system continuously reads the joint angles and performs real-time forward kinematics analysis to obtain the end-effector position. This information is transmitted to the Unity client via TCP/IP communication, enabling the mapping of the end-effector position of a robot onto the virtual hand model in the scene. The interactive feature is realised by touching the boxes with the virtual hand, simulating the action of grabbing a box. Moving the box to the designated numerical wall completes one placement action. This process is repeated for nine boxes, constituting one interactive training session. The scene is illustrated in Figure 14. The 3D effect is shown in Figure 15. The range of motion projection is depicted in Figure 16.

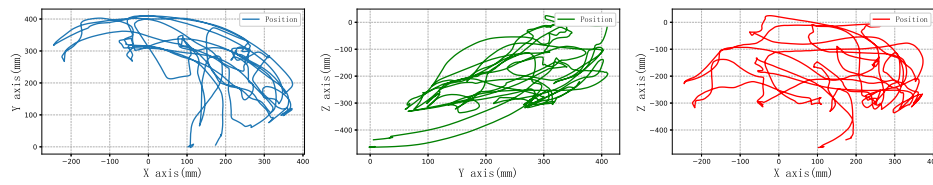


Figure 16. Range of motion projection.

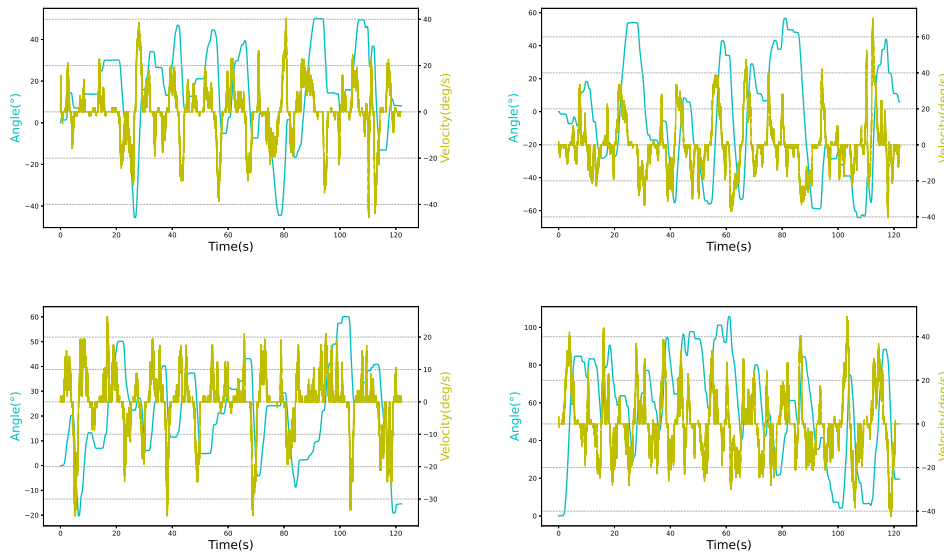


Figure 17. Virtual reality training movement data.

Table 6. Virtual reality training indicator evaluation table

	Max angle (deg)	Min angle (deg)	Max velocity (deg/s)	Min velocity (deg/s)
Joint1	50.15	-45.54	40.40	-45.69
Joint2	56.57	-64.22	70.30	-40.40
Joint3	60.10	-20.32	26.30	-35.20
Joint4	105.68	0.0	29.17	-42.17

Table 7. Joint angle/velocity diagram for gamified scenario training

	Joint1	Joint2	Joint3	Joint4
RMSE	0.973	1.224	1.489	0.881
MAE	0.791	0.986	1.124	0.786

By picking up the crates in different positions and placing them in the specified positions, the joint movement range of the patient can be trained in a wide range. The 3D effect diagram of the movement range is presented in Figure 15, and the projection of the movement trajectory in three planes is shown in Figure 16; the movement range of the human joint end can reach 616 mm in the X direction, 412 mm in the Y direction, and 488 mm in the Z direction. The magnitude of motion of the robot joint angles is shown in Figure 17. The kinematic moment data is displayed in Figure 18. The amplitude of motion of the first four joints during an interaction training session is demonstrated in Table 6.

The RMSE and MAE evaluation metrics are shown in Table 7. Through the above experiments, it can be

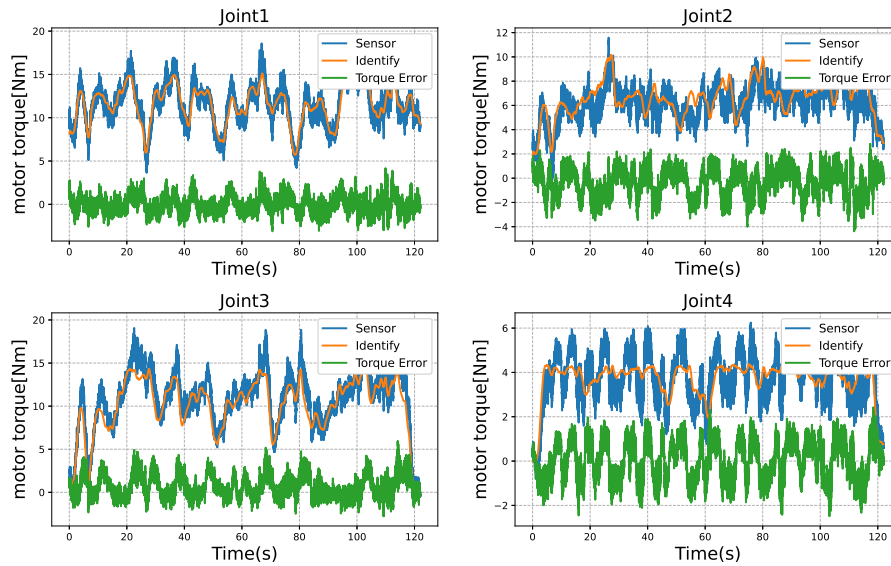


Figure 18. Virtual reality training moment data.

illustrated that the use of VR technology and the design of gamified scenes for active rehabilitation training have significant effects. Firstly, through visual feedback, intuitively completing the process of placing the wooden box can motivate patients to take the initiative to complete and enhance their motivation for rehabilitation; secondly, by setting the initial position of the wooden box in the gamified scene, the range of activities of the patient's motor rehabilitation can be adjusted according to the individual's rehabilitation situation. The method enhances the relevance and precision of rehabilitation training. Finally, during the execution of one rehabilitation training cycle, the movement moment curve of the patient is presented in Figure 18, and the average absolute error is shown in Table 7, with joints 1 and 4 less than 0.8 Nm, joint 2 less than 1 Nm, and joint 3 less than 1.2 Nm, which are in line with the rehabilitation training needs.

6. CONCLUSIONS

This paper proposes an active rehabilitation training method based on a 5-degree-of-freedom exoskeleton rehabilitation robot. Meanwhile, a gamified rehabilitation training program with a VR component is designed for upper limb rehabilitation. The robot modelling, including the MDH parameter table, kinematic rotation and position matrices calculation, is established first to achieve the passive training. The active rehabilitation method is built upon the traditional zero-force control algorithm by installing torque sensors at the robot joints, which can capture the interaction forces between the patient and the robot. An outer-loop PID control is designed to obtain the feedforward torque compensation values. This method can not only provide compensation torque for zero-force control but also address the issue of inaccurate dynamic models, so as to enhance system robustness. Furthermore, dynamic parameters are obtained through the dynamic identification method that uses a Fourier series excitation trajectory. The dynamics model obtained from the identification is used for the feedforward compensation function in passive training and the interactive force-assisted control in active training. In practical application, the fixed PID parameters may not be suitable for patients at different stages of rehabilitation; thus, a fuzzy control algorithm is designed. Fuzzy PID control demonstrates flexibility and robustness in active rehabilitation training, adapting well to nonlinearities and uncertainties, thereby improving system response speed and flexibility. Experiments show that the fuzzy control method reduces the RMSE and MAE evaluation indexes by more than 15% on average and improves the correlation coefficient by 4% compared with the traditional PID algorithm. Moreover, the new method effectively reduces the error surge phenomenon when torque commutation occurs. Finally, based on the proposed outer-loop

fuzzy PID-based active control method, a visually guided gamified rehabilitation training program is designed. This program enhances the efficiency of robot-assisted rehabilitation and makes it more interesting for patients in traditional rehabilitation training due to the monotonous training environment.

DECLARATIONS

Authors' contributions

Made substantial contributions to the conception and design of the study and performed data analysis and interpretation: Tong L, Cui D

Performed data acquisition and provided administrative, technical, and material support: Wang C, Peng L

Availability of data and materials

Not applicable.

Financial support and sponsorship

This work was supported by the National Key Research and Development Program of China under Grant 2022YFC3601200, the National Natural Science Foundation of China under Grant 62203441 and Grant U21A20479, and the Beijing Natural Science Foundation under Grant 4232053.

Conflicts of interest

All authors declared that there are no conflicts of interest.

Ethical approval and consent to participate

This research was reviewed and approved by the Ethics Committee of the Institute of Automation, Chinese Academy of Science (approval number: IA21-2309-020201). Written informed consent was signed by each subject prior to inclusion in the study.

Consent for publication

Not applicable.

Copyright

© The Author(s) 2024.

REFERENCES

1. Raina P, Gilsing A, Mayhew AJ, Sohel N, van den Heuvel E, Griffith LE. Individual and population level impact of chronic conditions on functional disability in older adults. *PLoS ONE* 2020;15:e0229160. DOI
2. Wang F, Zhang S, Zhou F, Zhao M, Zhao H. Early physical rehabilitation therapy between 24 and 48 h following acute ischemic stroke onset: a randomized controlled trial. *Disabil Rehabil* 2022;44:3967-72. DOI
3. Scheib J, Höke A. Advances in peripheral nerve regeneration. *Nat Rev Neurol* 2013;9:668-76. DOI
4. Babaiasl M, Mahdioun SH, Jaryani P, Yazdani M. A review of technological and clinical aspects of robot-aided rehabilitation of upper-extremity after stroke. *Disabil Rehabil* 2016;11:263-80. DOI
5. Li B, Li G, Sun Y, Jiang G, Kong J, Jiang D. A review of rehabilitation robot. In: 2017 32nd Youth Academic Annual Conference of Chinese Association of Automation (YAC); 2017 May 19-21; Hefei, China. IEEE; 2017. pp. 907-11. DOI
6. Hogan N, Krebs HI, Charnnarong J, Srikrishna P, Sharon A. MIT-MANUS: a workstation for manual therapy and training. I. In: Proceedings IEEE International Workshop on Robot and Human Communication; Tokyo, Japan. IEEE; 1992. pp. 161-5. DOI
7. Lum PS, Burgar CG, Van der Loos M, Shor PC, Majmundar M, Yap R. MIME robotic device for upper-limb neurorehabilitation in subacute stroke subjects: a follow-up study. *J Rehabil Res Dev* 2006;43:631-42. Available from: <https://pubmed.ncbi.nlm.nih.gov/7123204/>. [Last accessed on 7 Mar 2024]
8. Lum PS, Burgar CG, Shor PC, Majmundar M, Van der Loos M. Robot-assisted movement training compared with conventional therapy techniques for the rehabilitation of upper-limb motor function after stroke. *Arch Phys Med Rehab* 2002;83:952-9. DOI
9. Loureiro R, Amirabdollahian F, Topping M, Driessen B, Harwin W. Upper limb robot mediated stroke therapy - GENTLE/s approach. *Auton Robot* 2003;15:35-51. DOI

10. Maciejasz P, Eschweiler J, Gerlach-Hahn K, Jansen-Troy A, Leonhardt S. A survey on robotic devices for upper limb rehabilitation. *J Neuroeng Rehabil* 2014;11:3. [DOI](#)
11. Klamroth-Marganska V, Blanco J, Campen K, et al. Three-dimensional, task-specific robot therapy of the arm after stroke: a multicentre, parallel-group randomised trial. *Lancet Neurol* 2014;13:159-66. [DOI](#)
12. Nef T, Mihelj M, Colombo G, Riener R. ARMin - robot for rehabilitation of the upper extremities. In: Proceedings 2006 IEEE International Conference on Robotics and Automation; 2006 May 15-19; Orlando, USA. IEEE; 2006. pp. 3152-7. [DOI](#)
13. Kim B, Deshpande AD. An upper-body rehabilitation exoskeleton Harmony with an anatomical shoulder mechanism: design, modeling, control, and performance evaluation. *Int J Robot Res* 2017;36:414-35. [DOI](#)
14. Islam MR, Assad-Uz-Zaman M, Brahma B, Bouteraa Y, Wang I, Rahman MH. Design and development of an upper limb rehabilitative robot with dual functionality. *Micromachines* 2021;12:870. [DOI](#)
15. Huang J, Tu X, He J. Design and evaluation of the RUPERT wearable upper extremity exoskeleton robot for clinical and in-home therapies. *IEEE T Syst Man Cybern Syst* 2016;46:926-35. [DOI](#)
16. Lee HD, Lee BK, Kim WS, Han JS, Shin KS, Han CS. Human-robot cooperation control based on a dynamic model of an upper limb exoskeleton for human power amplification. *Mechatronics* 2014;24:168-76. [DOI](#)
17. Ball SJ, Brown IE, Scott SH. MEDARM: a rehabilitation robot with 5DOF at the shoulder complex. In: 2007 IEEE/ASME International Conference on Advanced Intelligent Mechatronics; 2007 Sep 04-07; Zurich, Switzerland. IEEE; 2007. p. 1-6. [DOI](#)
18. Brahma B, Saad M, Luna CO, Archambault PS, Rahman MH. Passive and active rehabilitation control of human upper-limb exoskeleton robot with dynamic uncertainties. *Robotica* 2018;36:1757-79. [DOI](#)
19. Ott C, Albu-Schaffer A, Kugi A, Stamiogioli S, Hirzinger G. A passivity based cartesian impedance controller for flexible joint robots - part I: torque feedback and gravity compensation. In: IEEE International Conference on Robotics and Automation; 2004 Apr 26 - May 01; New Orleans. IEEE; 2004. pp. 2659-65. [DOI](#)
20. Kim WS, Lee HD, Lim DH, Han JS, Shin KS, Han CS. Development of a muscle circumference sensor to estimate torque of the human elbow joint. *Sensor Actuat A Phys* 2014;208:95-103. [DOI](#)
21. Radke A, Gao Z. A survey of state and disturbance observers for practitioners. In: 2006 American Control Conference; 2006 Jun 14-16; Minneapolis, USA. IEEE; 2006. [DOI](#)
22. Rosen J, Brand M, Fuchs MB, Arcan M. A myosignal-based powered exoskeleton system. *IEEE Trans Syst Man Cybern A* 2001;31:210-2. [DOI](#)
23. Ison M, Artemiadis P. The role of muscle synergies in myoelectric control: trends and challenges for simultaneous multifunction control. *J Neural Eng* 2014;11:051001. [DOI](#)
24. Hashemi J, Morin E, Mousavi P, Mountjoy K, Hashtrudi-Zaad K. EMG-force modeling using parallel cascade identification. *J Electromyogr Kines* 2012;22:469-77. [DOI](#)
25. Khan AM, Yun D, Zuhair KM, et al. Estimation of desired motion intention and compliance control for upper limb assist exoskeleton. *Int J Control Autom Syst* 2017;15:802-14. [DOI](#)
26. Yin W, Sun L, Wang M, Liu J. Nonlinear state feedback position control for flexible joint robot with energy shaping. *Robot Auton Syst* 2018;99:121-34. [DOI](#)
27. Hu J, Xiong R. Contact force estimation for robot manipulator using semiparametric model and disturbance Kalman filter. *IEEE T Ind Electron* 2018;65:3365-75. [DOI](#)
28. Martinez S, Garcia-Haro JM, Victores JG, Jardon A, Balaguer C. Experimental robot model adjustments based on force-torque sensor information. *Sensors* 2018;18:836. [DOI](#)
29. Davari SA, Rodriguez J. Predictive direct voltage control of induction motor with mechanical model consideration for sensorless applications. *IEEE J Em Sel Top P* 2018;6:1990-2000. [DOI](#)
30. Chen S, Luo M, Jiang G, Abdelaziz O. Collaborative robot zero moment control for direct teaching based on self-measured gravity and friction. *Int J Adv Robot Syst* 2018;15:1729881418808711. [DOI](#)
31. Jin X, Chen K, Zhao Y, Ji J, Jing P. Simulation of hydraulic transplanting robot control system based on fuzzy PID controller. *Measurement* 2020;164:108023. [DOI](#)
32. Huang Y, Yasunobu S. A general practical design method for fuzzy PID control from conventional PID control. In: Ninth IEEE International Conference on Fuzzy Systems; 2000 May 07-10; San Antonio, USA. IEEE; 2000. pp. 969-72. [DOI](#)
33. Aprile I, Cruciani A, Germanotta M, et al. Upper limb robotics in rehabilitation: an approach to select the devices, based on rehabilitation aims, and their evaluation in a feasibility study. *Appl Sci* 2019;9:3920. [DOI](#)
34. Merat F. Introduction to robotics: mechanics and control. *IEEE J Robot Autom* 1987;3:166. [DOI](#)
35. Qin Z, Baron L, Birglen L. A new approach to the dynamic parameter identification of robotic manipulators. *Robotica* 2010;28:539-47. [DOI](#)
36. Atkeson CG, An CH, Hollerbach JM. Estimation of inertial parameters of manipulator loads and links. *Int J Robot Res* 1986;5:101-19. [DOI](#)
37. Swevers J, Verdonck W, De Schutter J. Dynamic model identification for industrial robots. *IEEE Contr Syst Mag* 2007;27:58-71. [DOI](#)
38. Jarrasse N, Proietti T, Crocher V, et al. Robotic exoskeletons: a perspective for the rehabilitation of arm coordination in stroke patients. *Front Hum Neurosci* 2014;8:947. [DOI](#)
39. Aguirre-Ollinger G, Colgate JE, Peshkin MA, Goswami A. Inertia compensation control of a one-degree-of-freedom exoskeleton for lower-limb assistance: initial experiments. *IEEE Trans Neural Syst Rehab Eng* 2012;20:68-77. [DOI](#)
40. Juang CF, Lai MG, Zeng WT. Evolutionary fuzzy control and navigation for two wheeled robots cooperatively carrying an object in

- unknown environments. *IEEE T Cybernetics* 2015;45:1731-43. DOI
41. Mirelman A, Patriiti BL, Bonato P, Deutsch JE. Effects of robot-virtual reality compared with robot alone training on gait kinetics of individuals post stroke. In: *2007 Virtual Rehabilitation*; 2007 Sep 27-29; Venice, Italy. IEEE; 2007. pp. 65-9. DOI